Environmental Science and Pollution Research
https://doi.org/10.1007/s11356-021-15339-7

RESEARCH ARTICLE

Influences of offshore background wind on the formation of sea-land breeze and the characteristics of pollutant diffusion

Jiajia Xu[1] · Hongwei Jia[1] · Huayuan Zhou[1] · Yanming Kang[1] · Ke Zhong[1]

Received: 20 January 2021 / Accepted: 3 July 2021

Abstract

The formation of sea-land breeze (SLB) is primarily affected by background wind and temperature difference between the sea and nearby land. Because the intensity of sea breeze is significantly stronger than that of land breeze, land breeze may result in more accumulated pollutants under the condition of offshore background wind (OBW) than under the condition of no OBW in coastal areas. The formation process of sea-land breeze and the dispersion trajectory and accumulation effect of pollutants are studied under different velocities of OBW with the same sea-land temperature difference by employing computational fluid dynamics (CFD). The results reveal that the depth and the duration of sea breeze decrease with the increase of the velocity of OBW. The most unfavorable velocity of OBW (0.2 m s^{-1}) exists when the concentration affected by OBW is higher than that by no OBW in coastal areas. The pollutants close to the ground will be blown to the inland by sea breeze when the velocity of OBW is less than 1.0 m s^{-1}. When the velocity of OBW is larger than 2.0 m s^{-1}, the pollutants will not occur on the inland due to the influence of OBW.

Keywords Sea-land breeze · Offshore background wind · Sea-land temperature difference · Pollutant accumulation · Inland distance · The most unfavorable velocity

Introduction

High-polluting industrial factories are usually built near coastline since the cost of shipping is much lower than that of land transportation (Tong et al. 2013). The pollutant transportation is affected by sea-land breeze (SLB) (Puygrenier et al. 2005; Bei et al. 2018), which originates from the local circulation with daily cycle, due to the sea-land temperature difference (Wenshi et al. 2001; Shen et al. 2019). Approximately 50% of population around the world lives within 50 km of the coastline (Pokhrel and Lee 2011), where the atmospheric pollution concentration is high due to the repeated accumulation of pollutants in the coastal zone by SLB. Therefore, the effect of SLB on the transportation process of pollutants has received more and more attention (Liu and Chan 2002; Ding et al. 2004; Tong et al. 2013; Nie et al. 2020).

The formation of SLB is primarily affected by background wind and sea-land temperature difference, and background wind can determine the formation and characteristics of SLB (Arritt 1993). Since the intensity of sea breeze is significantly higher than that of land breeze (Wexler 1946; Yoshino et al. 1973), the pollutants may quickly spread or accumulated under the condition of different background wind velocities. Helmis et al. (1995) compared the influence of background winds in different directions on the intensity of SLB, and the results showed that the onset direction and time of sea breeze are related to the background wind. Liu and Chan (2002) conducted a field test study in Hong Kong and found that the pollutant transportation is mainly controlled by the sea breeze circulation when the background wind is weak, resulting in the serious accumulation of pollutants. In addition, Kallos's research (Kallos et al. 1993) showed that the most serious air pollution incidents in the Athens area occurred when the synoptic and SLB were balanced.

The environmental aggravation caused by both OBW and SLB has received much attention, but few related studies have

Responsible Editor: V. V.S.S. Sarma

✉ Yanming Kang
ymkang@dhu.edu.cn

✉ Ke Zhong
zhongkeyx@dhu.edu.cn

[1] School of Environmental Science and Engineering, Donghua University, Shanghai 201620, China

Published online: 16 July 2021

been found. The possible reasons may be that the variables, OBW and sea-land temperature difference, cannot be separated by the common methods (e.g., field test and numerical simulations such as Weather Research and Forecasting (WRF) model). Therefore, previous studies only analyzed the characteristics of sea-land breeze and pollutant transportation under the coupling effect of both OBW and sea-land temperature difference.

Due to the fact that field test usually requires high economic cost, and the obtained data are limited, numerical simulation is thus becoming the primary method for SLB research. Lu and Turco (1994) studied the coupling effect between SLB and valley breeze under the condition of no background wind by using the three-dimensional hydrostatic primitive equation mesoscale model. With the improvement of computer performances and computational techniques, several softwares (e.g., WRF) have been developed and become the major tools for studying SLB (Zhen-zhou et al. 2014; Li and Chao 2016; Hai et al. 2018). For example, Ji et al. (2013) employed WRF to study the characteristics of sea breeze front development under different weather conditions in Korean Peninsula. However, the initial and boundary conditions of WRF are set as National Centers for Environmental Prediction (NCEP) Final analysis (FNL) data. Therefore, the influence of background wind and SLB on pollutant transportation cannot be separated from each other for analysis. In addition, the minimum computational grid (resolution) for WRF is 1 km (Ji et al. 2013), which is too large to explore the coupling effect between SLB and background wind.

To obtain an accurate flow field, computational grid needs to be refined to meter-level and smaller sizes by CFD techniques. Similarly, the boundary conditions for CFD can be set by user-defined functions, which is favorable for research by using control variable method. Recently, CFD has been applied in the fields of urban wind environment (Thaker and Gokhale 2016), evaluation of wind energy (Silva et al. 2015; Simões and Estanqueiro 2016), and wind field (Hacène et al. 2012; Liu et al. 2014), and the size of the flow field can be simulated gradually becomes large (Liu et al. 2017; Peng et al. 2018). This indicates that it is possible to set OBW as an independent variable to analyze the coupling effect between OBW and SLB and the pollutant transportation process by employing CFD method.

Therefore, the formation of SLB, and the transportation and cumulative effects of pollutants, is simulated by CFD under different velocities of OBW with the same sea-land temperature difference. Furthermore, the effects of OBW on the characteristics of SLB and pollutant transportation in coastal cities are explored to provide a reference for formulating the pollution control measures under different weather conditions.

Computational model and method verification

Governing equations

The airflow is regarded as a two-dimensional viscous flow to obtain explicit results. The mass and momentum conservation equations are expressed as follows:

$$\frac{\partial \overline{u}_i}{\partial x_i} = 0 \tag{1}$$

$$\frac{\partial \overline{u}_i}{\partial t} + u_j \frac{\partial \overline{u}_i}{\partial x_j} = -\frac{1}{\rho}\frac{\partial \overline{P}}{\partial x_i} - \frac{\partial \overline{u_i' u_j'}}{\partial x_j} + g_i \beta \left(\overline{T} - T_0\right) \tag{2}$$

and the energy equation can be written as

$$\frac{\partial \overline{T}}{\partial t} + \overline{u}_j \frac{\partial \overline{T}}{\partial x_j} = -\frac{\partial \overline{u_j' T'}}{\partial x_j} \tag{3}$$

where x_i and x_j are the Cartesian coordinates, the indices i and j range within values (1, 2), corresponding to (x, y) directions in space. $\overline{u}_i$ and g_i are the ith components of the mean velocity and the gravitational acceleration, respectively. Also, t is the time, ρ is the air density, β is the thermal expansion coefficient, and $\overline{P}$ and $\overline{T}$ are the mean pressure and the mean temperature, respectively. The terms u_i' and T' are the ith fluctuations of the velocity components and temperature, respectively. Finally, $\overline{u_i' u_j'}$ is the Reynolds stress tensor and $\overline{u_j' T'}$ is the turbulent heat flux.

Considering the influence of thermal effects on the air flow between sea and land, Boussinesq approximation is employed to address the buoyancy effect in momentum conservation. In this approximation, air density is treated as a constant value in all solved equations, except for the buoyancy term in momentum conservation (Mei et al. 2015), and the density variations can be expressed as temperature variations, i.e.,

$$\frac{\rho - \rho_0}{\rho_0} = -\beta\left(\frac{\overline{T} - T_0}{T_0}\right) \tag{4}$$

where ρ_0 and T_0 are the reference density and temperature. In the present study, T_0 = 20 °C, so the thermal expansion coefficient is about $\beta \sim 3 \times 10^{-3}$ (Kundu et al. 2016).

Different turbulence models can be applied to simulate the SLB and pollutant transportation. Comparing the Chen-Kim and RNG k-ε turbulence models with the wind tunnel measurements, Xie et al. (2005) found that the standard k-ε model is the most optimum turbulence model to obtain numerical results for air flow. It is then used to simulate the thermal effects on the flow field between sea and land. The commercial CFD code, Fluent 2019R1, is used to solve the Navier-

Stokes equations for the SLB using the standard k-ε turbulence model.

The standard k-ε turbulence model is a model based on model transport equations for the turbulent kinetic energy, k, and its dissipation rate, ε (ANSYS 2019). The turbulent kinetic energy k and its dissipation rate ε are calculated from the following semi-empirical transport equations (Hanjalic and Launder 1972).

Turbulent kinetic energy, k, is evaluated from

$$\frac{\partial k}{\partial t}+u_j\frac{\partial k}{\partial x_j}=\frac{\partial}{\partial x_j}\left(\frac{\nu_t}{\sigma_k}\cdot\frac{\partial k}{\partial x_j}\right)-\overline{u_i'u_j'}\cdot\frac{\partial \overline{u}_i}{\partial x_j}-g_i\beta\cdot\overline{u_i'T'}-\varepsilon \tag{5}$$

and the transport equation for turbulence dissipation rate, ε, is given as

$$\frac{\partial \varepsilon}{\partial t}+u_j\frac{\partial(\varepsilon)}{\partial x_j}=\frac{\partial}{\partial x_j}\left(\frac{\nu_t}{\sigma_\varepsilon}\cdot\frac{\partial \varepsilon}{\partial x_j}\right)-c_{\varepsilon,1}\frac{\varepsilon}{k}\nu_t\left(\overline{u_i'u_j'}\cdot\frac{\partial \overline{u}_i}{\partial x_j}+g_i\beta\cdot\overline{u_i'T'}\right)-c_{\varepsilon,2}\frac{\varepsilon^2}{k} \tag{6}$$

$$-\overline{u_i'u_j'}=\nu_t\left(\frac{\partial \overline{u}_i}{\partial x_j}+\frac{\partial \overline{u}_j}{\partial x_i}\right)-\frac{2}{3}k\delta_{ij} \tag{7}$$

$$-\overline{u_j'T'}=K_t\frac{\partial \overline{T}}{\partial x_j} \tag{8}$$

$$\nu_t=c_\mu\frac{k^2}{\varepsilon},\quad \mathrm{Pr}_t=\nu_t/K_t,\quad \beta=\frac{1}{V}\frac{\partial V}{\partial T}=-\frac{1}{\rho}\frac{\partial \rho}{\partial T} \tag{9}$$

where ν_t is the eddy viscosity, Pr_t is the turbulent Prandtl number, and δ_{ij} is the Kronecker delta.

The empirical modeling constants are set as the most commonly used values in industrial flow simulations, i.e., c_μ = 0.09, σ_ε = 1.0, σ_k = 1.3, $c_{\varepsilon,1}$ = 1.44, $c_{\varepsilon,2}$ =1.92, and Pr_t = 0.7.

In Fluent code, the mixing and transportation of pollutants can be modeled by solving conservation equations describing convection, diffusion, and reaction sources. The local mass fraction of pollutant, Y, is predicted through the solution of a convection-diffusion equation. The conservation equation can be expressed as

$$\frac{\partial}{\partial t}(\rho Y)+\nabla\cdot\left(\rho\overline{u}_i Y\right)=-\nabla\cdot\boldsymbol{J}+S \tag{10}$$

where $\boldsymbol{J}$ is the diffusion flux of pollutant, which arises due to gradients of concentration and temperature. S is the rate of creation by addition from the dispersed phase plus user-defined sources.

$$\boldsymbol{J}=-\left(\rho D_{i,m}+\frac{\mu_t}{Sc_t}\right)\nabla Y+D_{T,i}\frac{\nabla T}{T} \tag{11}$$

where $D_{\mathrm{i,m}}$ is the mass diffusion coefficient for species in the mixture, $D_{\mathrm{t,m}}$ is the thermal (Soret) diffusion coefficient, and Sc_t is the turbulent Schmidt number

$$Sc_t=\frac{\mu_t}{\rho D_t} \tag{12}$$

where μ_t is the turbulent viscosity and D_t is the turbulent diffusivity. In this CFD model, Sc_t = 0.7.

Computational domain, grid, and numerical scheme

Shanghai is located in the coastal area of east China plain to the west of East Sea with an average elevation of less than 50 m. Because Shanghai is not surrounded by any large mountain, SLB circulation could mainly influence the urban wind field. Figure 1a shows the topographic map of Shanghai. The largest industrial park of petrochemical industry is located at Jinshan District, Shanghai, only 3 km away from the south coastline. SLB greatly affects the transportation and diffusion characteristics of the emitted pollutants from the park. Because the large-scale circulation background will affect the development of SLB, the characteristics of SLB in the presence of background wind were studied in this paper. Since the intensity of the sea breeze is significantly higher than that of the land breeze, the existence of OBW will strengthen the land breeze, and further intensify the accumulation of pollutants in the coastal area. Consequently, the background wind is set as offshore type.

In the present study, the location of the industrial park is assumed as the emission source. To identify the basic characteristics of pollutant transport and diffusion influenced by both OBW and SLB, we consider the idealized configurations of a 60-km length of land (the white line in Fig. 1a) and a 60-km length of sea (the white line in Fig. 1a) with a vertical height of 5 km in two-dimensional mesoscale model. In addition, the results of previous studies showed that the influencing region of the building roof on airflow extended to about 3–5 times the height of the building (Franke 2006; Tominaga et al. 2008). Considering the height of numerous buildings in Shanghai are greater than 100 m, a 500-m-high drag reducing layer was set up to reflect the urban roughness layer, as shown in Fig. 1b.

The software ICEM 2019R1 is used to build the meshes for numerical simulation. A grid-independent analysis is carried out by constructing a set of quadrilateral-based structured grids with different grid numbers. The grid number is increased until the numerical results will not be affected by the grid size. A root-mean-square error of less than 2% for velocity is used as the criterion for grid independence in the present study, i.e.,

$$\sqrt{\frac{1}{N}\sum_{1}^{N}\left(\frac{V_m-V_{m-1}}{V_m}\right)^2}<0.02 \tag{13}$$

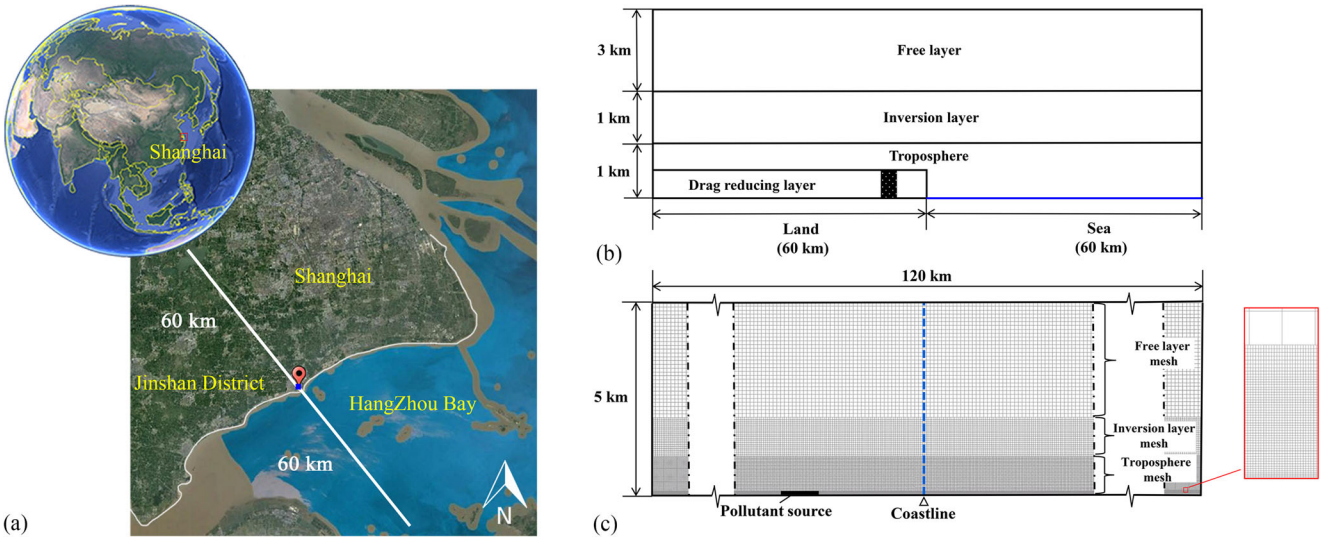

Fig. 1 Computational domain. (a) A topographic map of Shanghai. (b) Diagram of computational domain. (c) Grid of computational domain

where V_m is the velocity in the mth grid, $V_{m\text{-}1}$ is the velocity in the (m-1)th grid, and N is the number of the examined sample points.

The grid independence is achieved for velocity, and the height of the cells closest to the ground is 2 m, as shown in Fig. 1c. This mesh resolution is fine enough to ensure independent results, and the total number of the cells for the simulation is around 3.3 million.

A second-order upwind discretization scheme is used for most of the transport (i.e., the energy, momentum, k and ε) equations to reduce numerical diffusion and increase the computational accuracy, and the SIMPLE algorithm is adopted to couple pressure and velocity. PRESTO! is used for the spatial discretization of pressure because it is the most suitable scheme for calculating natural convection.

Boundary conditions and simulation preparation

The turbulence characteristics and the vertical speed profile of OBW are influenced by the type of terrain and it is an exponential function of terrain roughness. Because the depth of the urban atmospheric boundary layer is generally 800 m in Shanghai, the velocity of OBW over 800 m is assumed to be constant. Then the vertical speed profile of OBW is given by

$$V_y = V_r \times \left(H_y/H_r\right)^{\alpha} \qquad H_y < 800\ m \tag{14a}$$

$$V_y = V_r \times \left(800/H_r\right)^{\alpha} \qquad H_y \geq 800\ m \tag{14b}$$

where V_y and V_r are mean velocity at the height of H_y (m s^{-1}) and the reference height (m), respectively, H_y and H_r are the height from the ground (m) and the reference height (m), respectively, and α is the wind profile exponent. In the present study, α = 0.28 (Cheng et al. 2009; Oke et al. 2017), H_r = 10 m.

Four cases with different reference velocities, i.e., V_r = 0, 0.2, 1.0, and 2.0 m s^{-1}, are investigated by the numerical model, respectively, with the results shown in Fig. 2a. Free outflow boundary condition is applied on both lateral sides of the domain in the case of V_r = 0 m s^{-1}, whereas the left side (next to land) of the domain is treated as velocity inlet type, and the right side (next to sea) is regarded as outflow type in the case of OBW (i.e., V_r = 0.2, 1.0, and 2.0 m s^{-1}). The OBW profile is technically implemented via the user-defined function.

Inlet values of the turbulent kinetic energy (k_0) and its dissipation rate (ε_0) are specified as follows:

$$k_0 = \lambda\left(V_y\right)^2 \tag{15}$$

$$\varepsilon_0 = c_{\mu}^{3/4}\frac{k_0^{3/2}}{\kappa H_y} \tag{16}$$

where λ is the turbulent intensity, $\lambda = 3.0 \times 10^{-2}$, and κ is the Von Karman constant, κ = 0.41.

Slip wall with zero shear is imposed on the upper boundary. Non-slip for wall shear stress is applied on the bottom of the domain. In addition, a 500-m-high drag reducing layer is employed to simulate the urban roughness layer. The inertial resistance of the drag reducing layer is a function of the height from the ground, and it can be expressed by

$$C_{ir} = 5 \times 10^{-7} H_y + 0.0003 \tag{17}$$

The quantitative method is adopted to convert the actual land energy changes caused by solar radiation into a heat source. A time-varying intensity of heat source is used to achieve the temperature variation of the land surface affected by solar radiation or sky radiation. Figure 2b shows the time-varying intensity of heat source on the surface of land. The daily variation of seawater temperature is usually small because of the relatively large specific heat capacity of seawater,

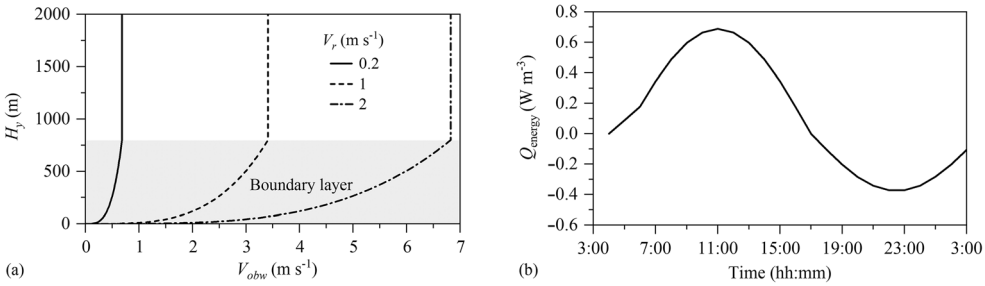

Fig. 2 Boundary conditions for inlet and heat source. (a) Offshore background wind velocity profiles. (b) Time series of heat source intensity on the surface of land in 1 day

leading to that the heating and cooling effects of the seawater on the air can be ignored and the surface of the sea is considered as a zero heat source during the simulation.

Based on the surface meteorological data and ERA5 hourly data (the fifth-generation ECMWF reanalysis for the global climate and weather) in 2015, a significant SLB was observed under stable weather on April 21, 2015. Therefore, the SLB is simulated using the quantitative method by Fluent 2019R1 based on the weather conditions of this day. To validate the simulation results, ERA5 hourly data at the height of 10 m and the simulation are compared on this day. As shown in Fig. 3, the results indicate that the cross-shore wind component u and temperature of the simulation show good agreement with the ERA5 hourly data under the condition of V_r = 0 m s^{-1}. Therefore, Fluent 2019R1 successfully reproduces the process of the sea-land breeze.

The initial velocity of the entire domain is 0 m s^{-1}, and the initial temperature over land and sea is set to be 20 °C. To avoid the influence of initial fields on numerical results, pre-simulation was carried out for several consecutive days under the same weather conditions to obtain the periodically varying flow and temperature fields at first. Figure 4a shows the time series of wind velocity at the height of 10 m and 1 km away from the coastline over land under the condition of V_r = 0.2 m s^{-1}. Figure 4b shows the time series of the average air temperature over land and the sea at the height of 100 m for V_r = 0.2 m s^{-1}. A 24-h periodicity can be observed in the flow and temperature field on the third day, and these fields are regarded as initial fields for transient calculations. Furthermore, the variation of temperature is consistent with the monitored data.

The pollutants released in the morning are more likely to transport and diffuse to the land by sea breeze formed around 9:00, which significantly affects the air quality in urban areas. Therefore, this study focuses on the spatiotemporal characteristics of pollutants released before the formation of sea breeze. The pollutants are assumed to be released from 8:00 to 8:30. A surface source of pollutants is placed on the land area, 3 km away from the south coastline, the size of pollutant source is 1000 m (width) × 100 m (height), and the emission rate of the pollutants, I, was 36 kg h^{-1}.

Results and discussions

The influence of offshore background wind on the characteristics of sea-land breeze

Figure 5 depicts the velocity vector with and without OBW at 9:00 and 17:00. It can be seen from Fig. 5a and b that an obvious sea breeze forms near the ground at 9:00, and it moves to inland area for about 20 km from the south coastline under the condition of no OBW. When the value of V_r is 1.0 m s^{-1}, only slight sea breeze forms on the coastline. This is because that the direction of OBW is opposite to that of sea breeze, hindering the formation and development of sea breeze.

With the increase of solar radiation intensity, the sea-land temperature difference increases, and the highest sea breeze intensity occurs at 17:00. The results in Fig. 5c and 5d show that the sea breeze front reaches the inland region more than 40 km in the case of no OBW and only 20 km in the case of V_r = 1.0 m s^{-1}. The depth of the sea-breeze layer and air flow velocity in the case of V_r = 1.0 m s^{-1} are significantly smaller than that under the condition of no OBW.

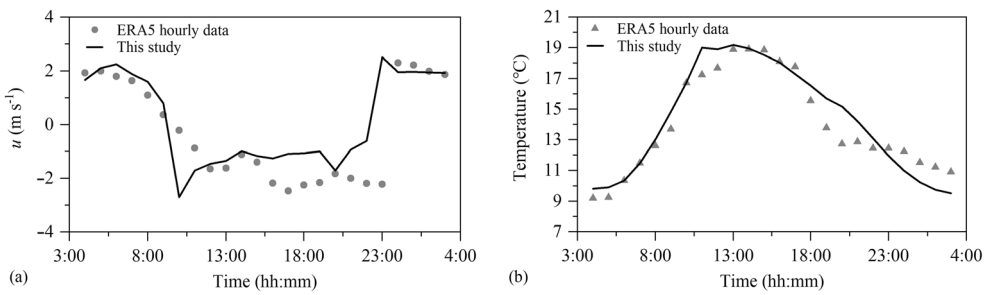

Fig. 3 Comparison of the simulation results with ERA5 hourly data. (a) Time series of cross-shore wind component u at the height of 10 m. (b) Time series of the temperature at the height of 10 m

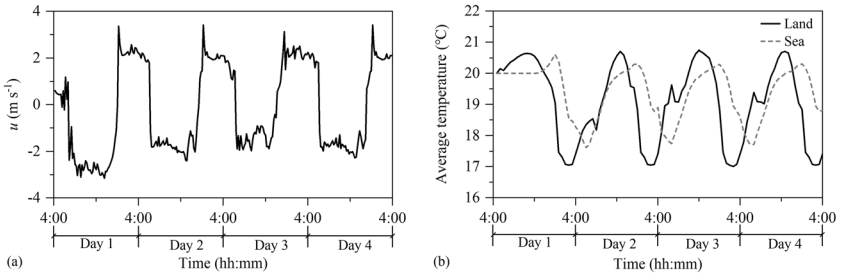

Fig. 4 Time series of cross-shore wind component u and the average air temperature in a pre-simulation. (a) Time series of cross-shore wind component u at the height of 10 m and 1 km away from the coastline over land. (b) Time series of the average air temperature over land and sea at the height of 100 m under the condition of $V_r = 0.2$ m s^{-1}

The depth of the sea breeze and land breeze

The depth of the sea-land breeze, as well as its beginning, end, and duration, is important characteristics of SLB (Zhong and Takle 1992). Figure 6 presents the distribution of the cross-shore wind velocity component (u) along the height with and without OBW. It should be noted that when the wind blows from the land to the sea, $u > 0$ m s^{-1}, otherwise $u < 0$ m s^{-1}.

It can be seen from Fig. 6a and 6b that the wind profile during the sea breeze period is near the ground regardless of the presence of OBW. The wind blows from the sea to the land near the ground ($u < 0$ m s^{-1}) and blows from the land to the sea ($u > 0$ m s^{-1}) at the high altitude, forming the sea breeze circulation. The wind profile during the land breeze period (Fig. 6c and d) is opposite to that during the sea breeze period, forming the land breeze circulation.

Comparing Fig. 6a and 6b, the sea breeze velocity near the ground without OBW is shown to be significantly higher than that with OBW due to the influence of the OBW; the former is about 3.5 m s^{-1} and the latter is about 2.0 m s^{-1}. In addition, the velocities of the return flow with and without OBW at the high altitude are different from that near the ground. It can also be seen from Fig. 6c and 6d that OBW significantly increases the land breeze velocity, and the maximum velocity near the ground without OBW is only 1/2 to 1/3 of that with OBW. This is because that the direction of the OBW is opposite to the direction of the sea breeze and same as the direction of the sea breeze return flow and land breeze. The coupling effect can increase the wind speed and strengthen the intensity of land breeze.

The depth of SLB is an important index of the intensity of SLB. Hence, $u = 0$ m s^{-1} is used as the criterion to determine the depth of SLB in this study. By analyzing the numerical results of OBW at 0 m s^{-1}, 0.2 m s^{-1}, 1.0 m s^{-1}, and 2.0 m s^{-1}, the hourly variation of the SLB depth is shown in Fig. 7.

The results in Fig. 7a show that the depth of the sea breeze (DSB) can be up to 1 km during the strongest sea breeze period under the condition of no OBW. At other moments, it varies in the range of which is consistent with the radar observation results summarized by Ma et al. (2021).

Figure 7 also indicates that the depth of the land breeze (DLB) is only 200 m, which is much less than DSB. The intensity of the land breeze is significantly less than that of the sea breeze, which is consistent with the results of the previous study (Wexler 1946; Yoshino et al. 1973). When the value of V_r is 0.2 m s^{-1} (Fig. 7b), the generation of the OBW reduces the maximum DSB and shortens the transition period and the land-breeze period that can be identified. Comparing Fig. 7b to 7d, it can be observed that DSB decreases sharply from 800 m to tens of meters as V_r increases from 0.2 to 2.0 m s^{-1}.

In addition, when the OBW velocity is high, the proportion of the night-time offshore wind caused by the sea-land temperature difference will be reduced, and this will result in errors in the calculation of DLB, so the land breeze depth is not given in Fig. 7c and 7d.

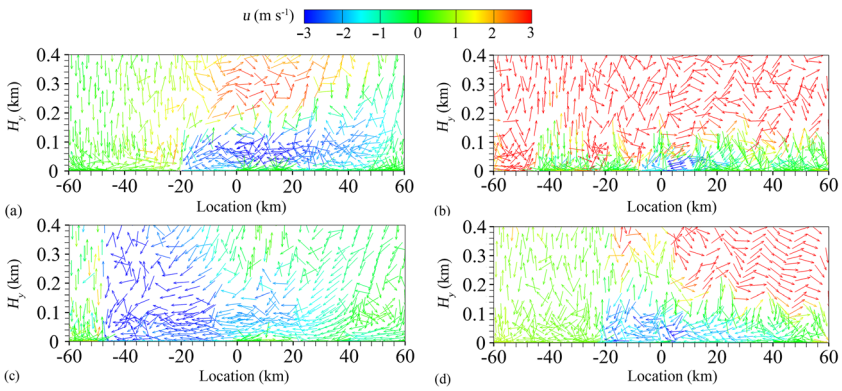

Fig. 5 Velocity vector of the entire domain. (a) $V_r = 0$ m s^{-1}, the onset of sea breeze (9:00). (b) $V_r = 1.0$ m s^{-1}, the onset of sea breeze (9:00). (c) $V_r = 0$ m s^{-1}, the strongest sea breeze (17:00). (d) $V_r = 1.0$ m s^{-1}, the strongest sea breeze (17:00)

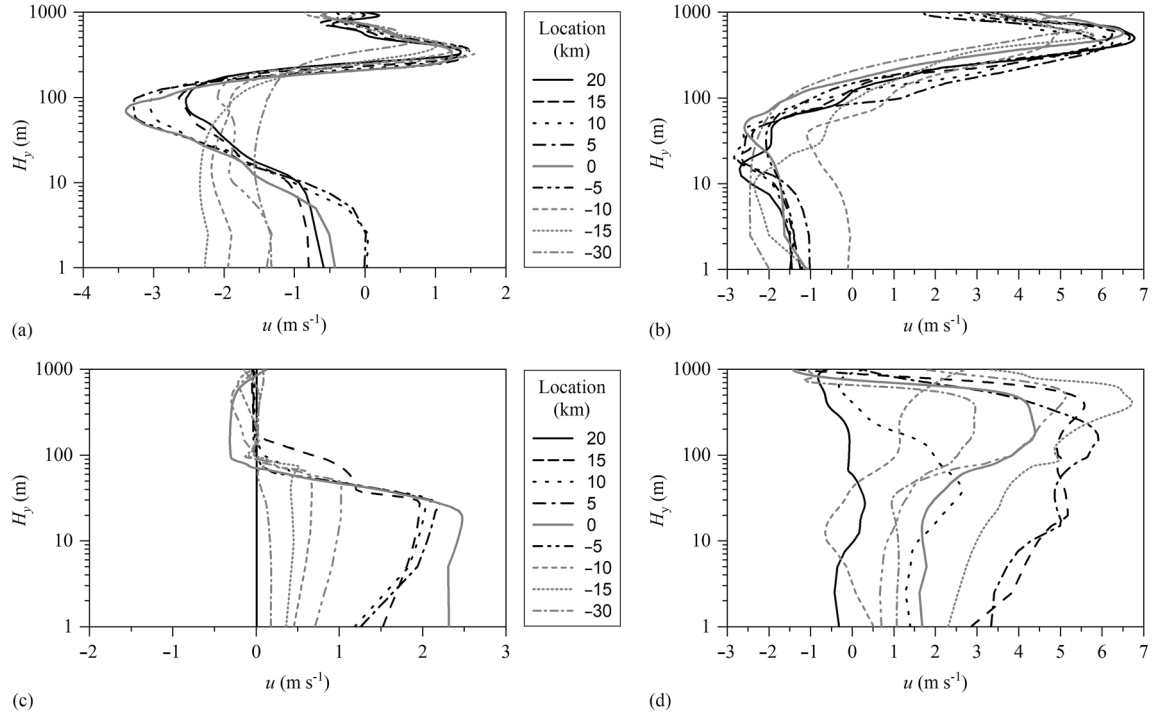

Fig. 6 Predicted profiles of cross-shore wind component in different locations. (a) V_r = 0 m s^{-1}, sea-breeze period (12:00). (b) V_r = 1.0 m s^{-1}, sea-breeze period (12:00). (c) V_r = 0 m s^{-1}, land-breeze period (23:00). (d) V_r = 1.0 m s^{-1}, land-breeze period (4:00)

The duration of sea breeze and land breeze

Figure 8 provides the beginnings and the ends of sea breeze, land breeze, and transition periods under different values of V_r. The results show that the beginning and the end of sea breeze period is gradually postponed and advanced, respectively, with the increase of OBW speed. For instance, the sea breeze starts at around 7:30 and 10:00 for the cases of $V_r \leq 0.2$ m s^{-1} and V_r = 2.0 m s^{-1}, respectively, and the time difference is about 150 min. Two possible reasons lead to this phenomenon. One is that OBW will blow the warm air from the land to the sea during the daytime, thereby reducing the sea-land temperature difference and postponing the beginning of sea breeze. The other is that the direction of OBW is opposite to that of the sea breeze. On the other hand, the sea breeze ends at around 20:40 and 17:40 in the cases of $V_r \leq 0.2$ m s^{-1} and V_r = 2.0 m s^{-1}, respectively. The end of the sea breeze with OBW is 3 h earlier than that without OBW. This is because that the sea breeze is slight under the condition of high V_r and can be significantly affected by the OBW.

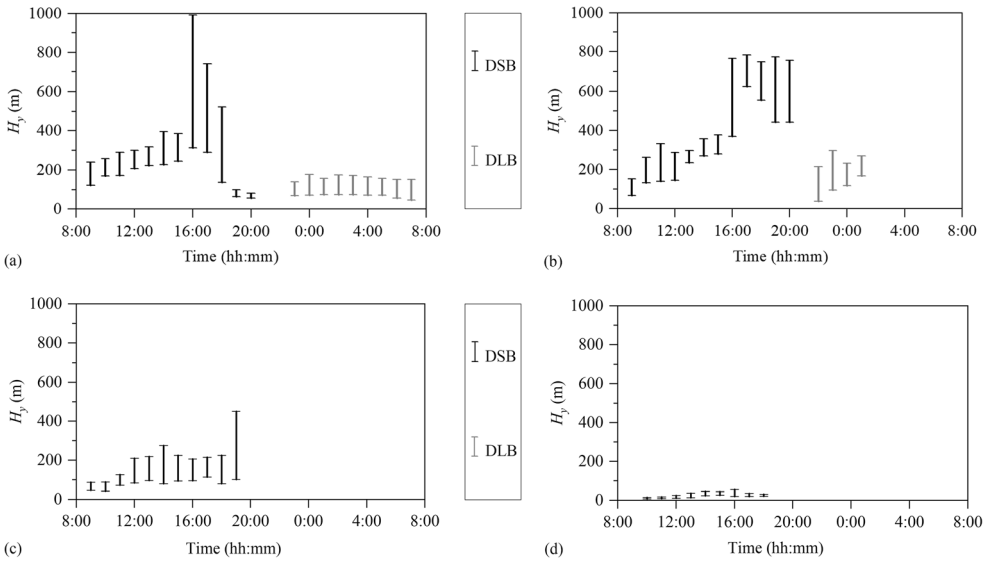

Fig. 7 DSB and DLB under different offshore background wind velocities. (a) V_r = 0 m s^{-1}. (b) V_r = 0.2 m s^{-1}. (c) V_r = 1.0 m s^{-1}. (d) V_r = 2.0 m s^{-1}

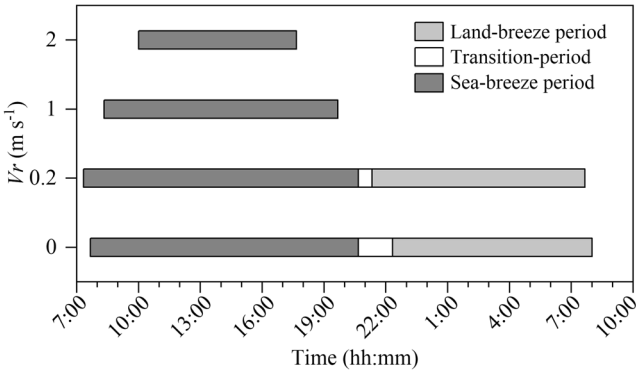

Fig. 8 Durations of sea-breeze and land-breeze under different offshore background wind velocities

It can also be found that OBW in the case of $V_r = 0.2$ m s^{-1} accelerates the transition process from sea breeze to land breeze, and the conversion time is reduced by about 1 h compared with the condition of no OBW.

Impact of both background wind and sea-land breeze on the pollutant transportation

The dimensionless concentration of pollutants (C_p^*) is defined by

$$C_p^* = C_p / \left(\frac{I \times \tau}{V_{vol}} \right) \tag{18}$$

where C_p is the concentration of pollutants (kg m^{-3}), I is the emission rate of the pollutants (kg s^{-1}), τ is the duration time of releasing pollutants (s), and V_{vol} is the volume of the domain (m^3).

Previous studies showed that the interaction of OBW and SLB has a significant effect on air pollution (Liu and Chan 2002; Ding et al. 2004; Tong et al. 2013; Nie et al. 2020). Figure 9 presents the dimensionless concentration of pollutants (C_p^*) when the value of V_r is 0 m s^{-1} and 1.0 m s^{-1}, respectively. It should be noted that the pollutant release time is set at 8:00−8:30 (before the beginning of sea breeze).

Figure 9a and 9b show that the pollutant concentration over land near the coastline is reduced by the clean air from the sea. However, the inland area is heavily polluted due to the sea breeze close to the ground (Fig. 9d and 9e), and the position of heavy pollution is almost the same as the sea breeze front. The pollutants follow the return flow and reach a stagnant state above the sea which exceeds the height that can be affected by SLB circulation under the weather condition (Fig. 9f). The pollutants will accumulate at high altitude in the case of no OBW.

Although the sea breeze affected by OBW is relatively slight, some pollutants will transport to the inland near the ground when the velocity of OBW is 1.0 m s^{-1} (Fig. 9j and 9k). The pollutants at the high altitude are mainly affected by OBW, and transport to the open sea, and the accumulation effect of pollutants is slight.

Spatial variation of pollutants

The time series of C_p^* along the cross-shore direction at the height of 10 m are shown in Fig. 10.

It can be observed from Fig. 10 that the range of pollutants expands over time and the peak concentration gradually decreases regardless of the value of V_r. However, the spatiotemporal distributions of pollutant concentration significantly change with the value of V_r.

When the value of V_r is relatively small (Fig. 10a and 10b), the coastal pollutants released in the morning will only spread to the land near ground during the daytime (before 19:00). However, the direction of pollutant transportation, which is from land to sea, is primarily dominated by OBW when the value of V_r reaches 2.0 m s^{-1} (Fig. 10d).

The direction of pollutant transportation will change around 13:00 when the value of V_r is 1.0 m s^{-1} (Fig. 10c). The pollutants only spread to the land before 13:00, and then the pollutants spread to both the land and the sea. In particular, not only the range of pollutant becomes larger, but also the pollutant concentration will be higher at 19:00 and 21:00. This is because the pollutants that have been transported to the inland will return to the near coast land and the sea with the land breeze.

Comparing Fig. 10a to Fig. 10d, it can be found that the pollutants gradually move to inland over time during the sea breeze period regardless of the values of V_r, but the range affected by pollutant depends on the velocity of OBW. The maximum distance that the pollutants can affect the land is only about 15 km from the coastline in the case of $V_r = 2.0$ m s^{-1}. When the value of V_r is 0, 0.2, and 1.0 m s^{-1}, the time that the pollutant reaches 60 km inland is 17:00, 19:00, and 21:00 with the duration of 9, 11, and 13 h, respectively. The sea breeze is the driving force for the pollutants moving to inland, while the OBW is in the opposite direction of the sea breeze, which hinders the development of the sea breeze.

Temporal variation of pollutants

To analyze the polluting levels in different regions, the area investigated in the present study is divided into four sub-areas, including the land area near the coastline (land 1), the pollution source area (land 2), the land area away from the coastline (land 3), and the sea area (sea). Figure 11 presents the variations of C_p^* in the four regions within 100 m above the ground and the entire domain.

The results in Fig. 11 show that the pollutant concentration in all the four sub-regions decreases and then increases over time when V_r is ≤ 1.0 m s^{-1} (Fig. 11a to 11c). The possible reason is that the fully developed sea breeze circulation brings

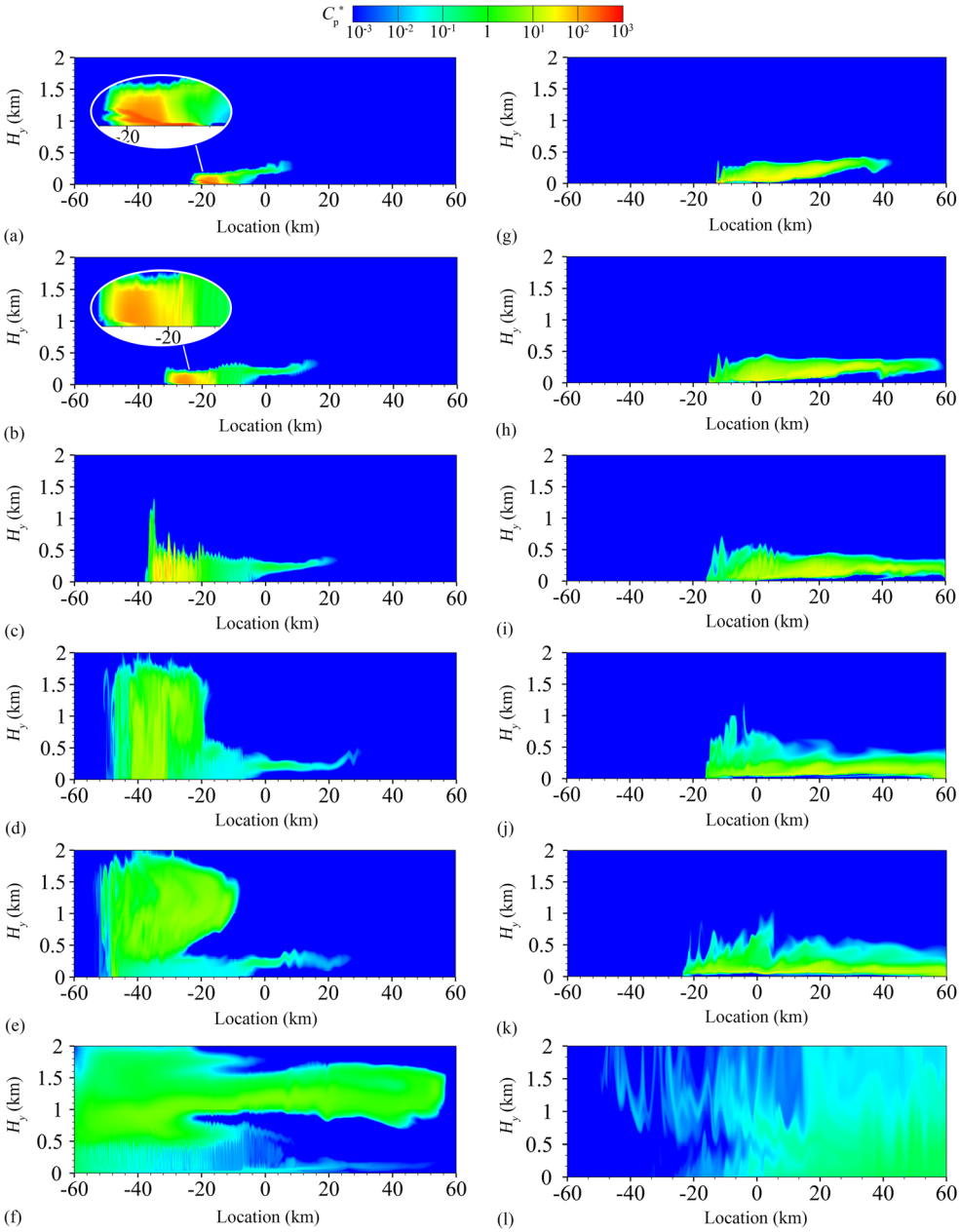

Fig. 9 Distribution of pollutants under different coupled offshore background wind with sea-land breeze. (a) V_r = 0 m s^{-1} at 10:00. (b) V_r = 0 m s^{-1} at 11:00. (c) V_r = 0 m s^{-1} at 12:00. (d) V_r = 0 m s^{-1} at 15:00. (e) V_r = 0 m s^{-1} at 17:00. (f) V_r = 0 m s^{-1} at 9:00 (next day). (g) V_r = 1.0 m s^{-1} at 10:00. (h) V_r = 1.0 m s^{-1} at 11:00. (i) V_r = 1.0 m s^{-1} at 12:00. (j) V_r = 1.0 m s^{-1} at 15:00. (k) V_r = 1.0 m s^{-1} at 17:00. (l) V_r = 1.0 m s^{-1} at 9:00 (next day)

the pollutants to the upper air and reduces the concentration near the ground. However, the sea breeze circulation will be destroyed and the pollutants in the upper air will return to the near ground during the transition period. When the value of V_r reaches to 2.0 m s^{-1}, the pollutant concentrations in all the five regions only decrease due to the excessive velocity of OBW.

Comparing Fig. 11a to d, it can be observed that the pollutant concentration under the condition of V_r = 0.2 m s^{-1} is the highest (even higher than that when V_r = 0 m s^{-1}). This indicates that OBW has the most unfavorable value for the pollutant transportation. It is important to determine the specific range of the most unfavorable velocity for the early warning of air pollution and the control of pollutant emissions. Therefore, the specific range of the most unfavorable velocity needs to be investigated in further study.

Conclusions

The influences of offshore background wind (OBW) on the formation of sea-land breeze (SLB) and the characteristics of pollutants diffusion in coastal cities are simulated by employing CFD techniques. The main conclusions are as follows:

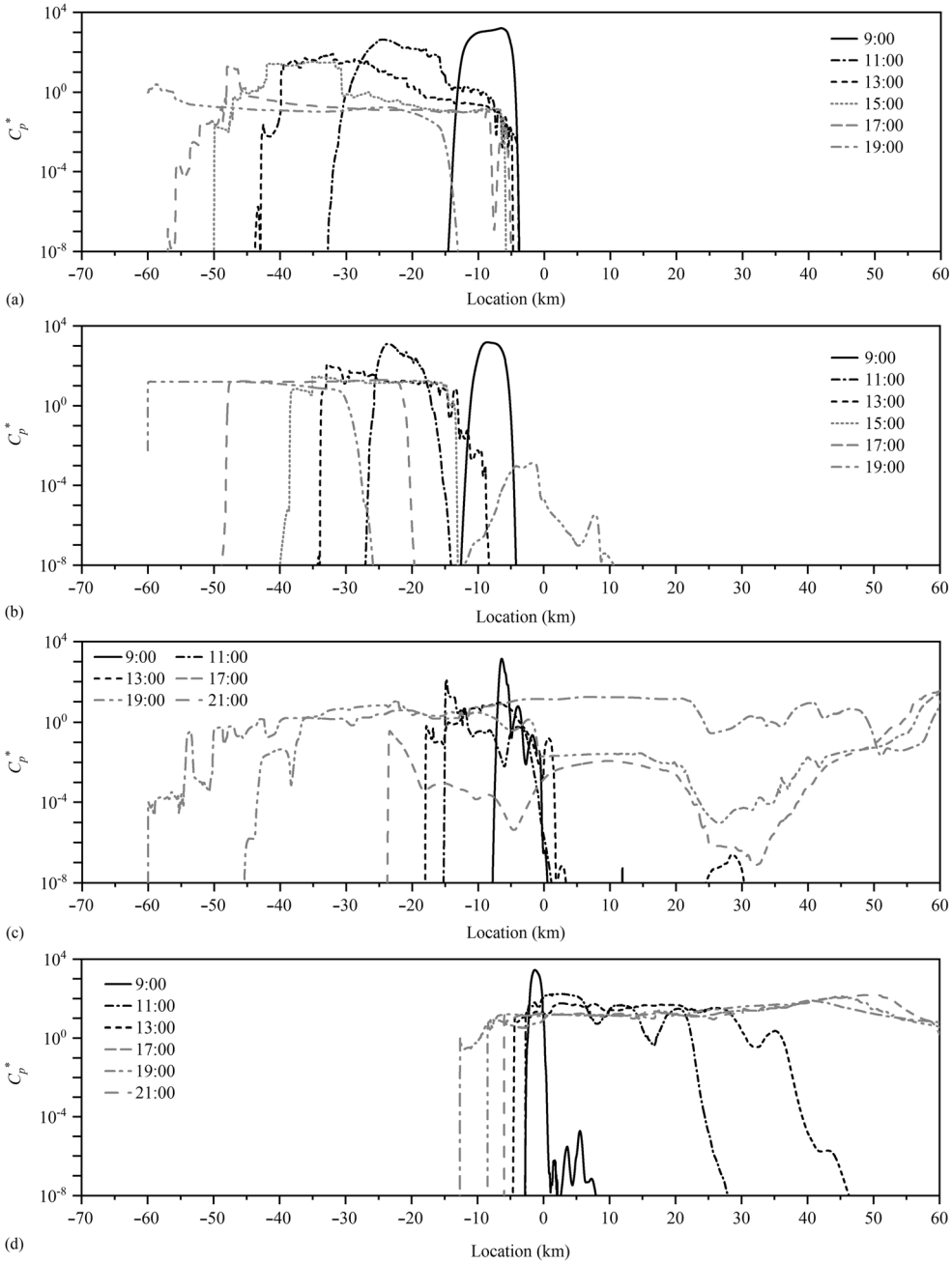

Fig. 10 Distribution of pollutants at H_y = 10 m under different offshore background wind velocities. (a) V_r = 0 m s^{-1}. (b) V_r = 0.2 m s^{-1}. (c) V_r = 1.0 m s^{-1}. (d) V_r = 2.0 m s^{-1}

1. The depth of sea breeze (DSB) and land breeze (DLB) is significantly affected by OBW. DSB can reach hundreds of meters or even 1000 m under the condition of no OBW. DLB is lower than that of DSB, which is less than 200 m. With the increase of the velocity of OBW, DSB will decrease. When the value of V_r increases to 2.0 m s^{-1}, DSB is only tens of meters.
2. The existence of OBW will postpone the beginning of sea breeze and advance the end of sea breeze. The durations of sea breeze under the condition of V_r = 1.0 m s^{-1} and 2.0 m s^{-1} are shortened by around 1.7 h and 7.3 h, respectively, compared with that under the condition of V_r = 0 m s^{-1}.
3. The existence of OBW can hinder the inland transportation of pollutants caused by sea breeze. In the case of V_r = 2.0 m s^{-1}, the inland distance is small (only 15 km), whereas the inland distance can be up to 60 km for the case of no OBW.
4. When the value of V_r is small, land breeze may result in more accumulated pollutants under the condition of offshore background wind (OBW) than that under the condition of no OBW in coastal areas. In the present study, the value of V_r = 0.2

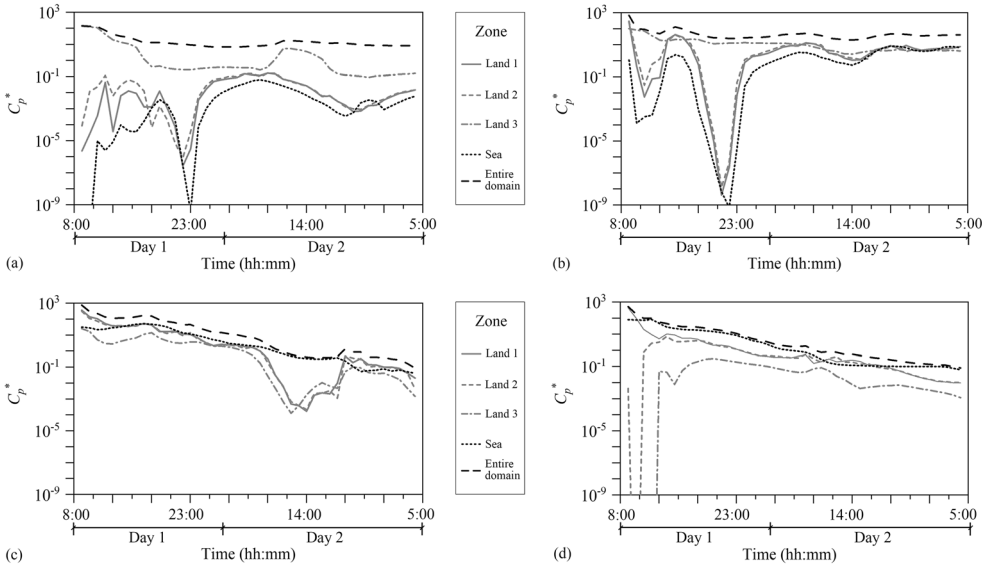

Fig. 11 Variations of C_p^* in typical zones under different offshore background wind velocities. (a) V_r = 0 m s^{-1}. (b) V_r = 0.2 m s^{-1}. (c) V_r = 1.0 m s^{-1}. (d) V_r = 2.0 m s^{-1}

m s^{-1} is the most unfavorable velocity for pollutant transportation on the SLB day.

Determining the specific range of the most unfavorable wind speed can provide a theoretical reference for formulating local pollutant emission standards. Due to the limited cases studied in this work, further research needs to be conducted to comprehensively explore the most unfavorable velocity.

Author contribution Jiajia Xu, she is the first author. She did all the simulation and finished the original writing of the manuscript.

Hongwei Jia, Dr. Jia is the co-investigator of this study.

Huayuan Zhou participated in analyzing the results and writing of the manuscript with the first author together.

Yanming Kang, Prof. Kang is the first corresponding author. He designed the research plan and helped the first author write the original manuscript.

Ke Zhong, Prof. Zhong is the co-corresponding author. She designed the research plan with Prof. Kang and analyzed the results with the first author.

Funding This work was supported by the Science and Technology Commission of Shanghai Municipality (Grant No. 19DZ1205005); the National Natural Science Foundation of China (Grant Nos. 42075179, 51578121); and the Fundamental Research Funds for the Central Universities (Grant No. CUSF-DH-D-2021040).

Data availability All data generated or analyzed during this study are included in this published article.

Declarations

Ethics approval and consent to participate Not applicable.

Consent for publication Not applicable.

Competing interests The authors declare no competing interests.

References

ANSYS 19.3 (2019) Fluent Theory Guide. ANSYS Inc.

Arritt RW (1993) Effects of the large-scale flow on characteristic features of the sea breeze. J Appl Meteorol 32:116–125

Bei N, Zhao L, Wu J, Li X, Feng T, Li G (2018) Impacts of sea-land and mountain-valley circulations on the air pollution in Beijing-Tianjin-Hebei (BTH): a case study. Environ Pollut 234:429–438

Cheng W, Liu C-H, Leung DY (2009) On the correlation of air and pollutant exchange for street canyons in combined wind-buoyancy-driven flow. Atmos Environ 43:3682–3690

Ding A, Wang T, Zhao M, Wang T, Li Z (2004) Simulation of sea-land breezes and a discussion of their implications on the transport of air pollution during a multi-day ozone episode in the Pearl River Delta of China. Atmos Environ 38:6737–6750

Franke J (2006) Recommendations of the COST action C14 on the use of CFD in predicting pedestrian wind environment. In: The fourth international symposium on computational wind engineering. Yokohama, Japan, pp 529–532

Hacène FB, Abbés MT, Merzouk NK, Loukarfi L, Mahmoudi H, Goosen MF (2012) Development of a simulation model for a three-dimensional wind velocity field using Ténès Algeria as a case study. Renew Sust Energ Rev 16:29–36

Hai S, Miao Y, Sheng L, Wei L, Chen Q (2018) Numerical study on the effect of urbanization and coastal change on sea breeze over Qingdao, China. Atmosphere 9:345

Hanjalic K, Launder B (1972) A Reynolds stress model of turbulence and its application to thin shear flows. J Fluid Mech 52:609–638

Helmis C, Papadopoulos K, Kalogiros J, Soilemes A, Asimakopoulos D (1995) Influence of background flow on evolution of Saronic Gulf sea breeze. Atmos Environ 29:3689–3701

Ji H-E, Lee S-H, Lee H-W (2013) Characteristics of sea breeze front development with various synoptic conditions and its impact on lower troposphere ozone formation. Adv Atmos Sci 30:1461–1478

Kallos G, Kassomenos P, Pielke RA (1993) Synoptic and mesoscale weather conditions during air pollution episodes in Athens, Greece. In: Transport and diffusion in turbulent fields. Springer, Dordrecht, pp 163–184

Kundu PK, Cohen IM, Cowling DR (2016) *Fluid mechanics*, 6th edn. Elsevier Inc., Oxford

Li Y, Chao J (2016) An analytical solution for three-dimensional sea–land breeze. J Atmos Sci 73:41–54

Liu H, Chan JC (2002) An investigation of air-pollutant patterns under sea–land breezes during a severe air-pollution episode in Hong Kong. Atmos Environ 36:591–601

Liu B, Qu J, Niu Q, Wang J, Zhang K (2014) Computational fluid dynamics evaluation of the effect of different city designs on the wind environment of a downwind natural heritage site. J Arid Land 6:69–79

Liu S, Pan W, Zhang H, Cheng X, Long Z, Chen Q (2017) CFD simulations of wind distribution in an urban community with a full-scale geometrical model. Build Environ 117:11–23

Lu R, Turco RP (1994) Air pollutant transport in a coastal environment. Part I: Two-dimensional simulations of sea-breeze and mountain effects. J Atmos Sci 51:2285–2308

Ma Y, Xin J, Zhang X, Dai L, Schaefer K, Wang S, Wang Y, Wang Z, Wu F, Wu X, Fan G (2021) Land–sea breeze circulation structure on the west coast of the Yellow Sea, China. Atmos and Oceanic Sci Letters 14:100003

Mei D, Deng Q, Wen M, Fang Z (2015) Evaluating dust particle transport performance within urban street canyons with different building heights. Aerosol Air Qual Res 16:1483–1496

Nie X et al (2020) Total gaseous mercury in a coastal city (Qingdao, China): influence of sea-land breeze and regional transport. Atmos Environ 235:117633

Oke T, Mills G, Christen A, Voogt J (2017) Urban climates. Cambridge University Press, Cambridge

Peng L et al (2018) Wind weakening in a dense high-rise city due to over nearly five decades of urbanization. Build Environ 138:207–220

Pokhrel R, Lee H (2011) Estimation of the effective zone of sea/land breeze in a coastal area. Atmos Pollut Res 2:106–115

Puygrenier V, Lohou F, Campistron B, Saïd F, Pigeon G, Bénech B, Serça D (2005) Investigation on the fine structure of sea-breeze during ESCOMPTE experiment. Atmos Res 74:329–353

Shen L, Zhao C, Ma Z, Li Z, Li J, Wang K (2019) Observed decrease of summer sea-land breeze in Shanghai from 1994 to 2014 and its association with urbanization. Atmos Res 227:198–209

Silva J, da Silva FM, Couto A, Estanqueiro A (2015) A method to correct the flow distortion of offshore wind data using CFD simulation and experimental wind tunnel tests. J Wind Eng Ind Aerodyn 140:87–94

Simões T, Estanqueiro A (2016) A new methodology for urban wind resource assessment. Renew Energy 89:598–605

Thaker P, Gokhale S (2016) The impact of traffic-flow patterns on air quality in urban street canyons. Environ Pollut 208:161–169

Tominaga Y, Mochida A, Yoshie R, Kataoka H, Nozu T, Yoshikawa M, Shirasawa T (2008) AIJ guidelines for practical applications of CFD to pedestrian wind environment around buildings. J Wind Eng Ind Aerodyn 96:1749–1761

Tong L, Liao X, Chen J, Xiao H, Xu L, Zhang F, Niu Z, Yu J (2013) Pollution characteristics of ambient volatile organic compounds (VOCs) in the southeast coastal cities of China. Environ Sci Pollut Res 20:2603–2615

Wenshi L, Anyu W, Chisheng W, Kun FS, Chimeng K (2001) A case modeling of sea–land breeze in Macao and its neighborhood. Adv Atmos Sci 18:1231–1240

Wexler R (1946) Theory and observations of land and sea breezes. Bull Am Meteorol Soc 27:272–287

Xie X, Huang Z, Wang J-S (2005) Impact of building configuration on air quality in street canyon. Atmos Environ 39:4519–4530

Yoshino M, Kudo T, Hoshino M (1973) Land and sea breezes on the coast of Japan Sea. Geogr Rev Jpn 46:205–210

Zhen-zhou Z, Chao-xiong C, Yu S, Ling K, Xu-hui C (2014) Statistical characteristics and numerical simulation of sea land breezes in Hainan island. J Trop Meteorol 20(3):267–278

Zhong S, Takle ES (1992) An observational study of sea-and land-breeze circulation in an area of complex coastal heating. J Appl Meteorol 31:1426–1438